




Article

Effect of Ag₂S Nanocrystals/Reduced Graphene Oxide Interface on Hydrogen Evolution Reaction

Chen Zhao ^{1,2}, Zhi Yu ¹, Jun Xing ^{1,2}, Yuting Zou ^{1,2}, Huiwen Liu ³, Hao Zhang ³, Weili Yu ^{1,2,*} , Hicham Idriss ^{4,*}  and Chunlei Guo ^{5,*} 

¹ The Photonics Laboratory, State Key Laboratory of Applied Optics, Changchun Institute of Optics, Fine Mechanics and Physics, Chinese Academy of Sciences, Changchun 130033, China; zhaochen16@mails.ucas.ac.cn (C.Z.); zhiyu@ciomp.ac.cn (Z.Y.); xingjun15@mails.ucas.edu.cn (J.X.); zouyuting16@mails.ucas.ac.cn (Y.Z.)

² University of Chinese Academy of Sciences, Beijing 100049, China

³ State Key Laboratory of Supramolecular Structure and Materials, College of Chemistry, Jilin University, Changchun 130012, China; liuhuiwenjlu@163.com (H.L.); hao_zhang@jlu.edu.cn (H.Z.)

⁴ SABIC-CRD, King Abdullah University of Science and Technology (KAUST), Thuwal 23955-6900, Saudi Arabia

⁵ The Institute of Optics, University of Rochester, Rochester, NY 14627, USA

* Correspondence: weili.yu@ciomp.ac.cn (W.Y.); h.idriss@ucl.ac.uk (H.I.); chunlei.guo@rochester.edu (C.G.)

† Current address: Department of Chemistry, University College London, London WC1E 6BT, UK.

Received: 23 June 2020; Accepted: 11 August 2020; Published: 19 August 2020



Abstract: The development of efficient electrocatalyst to produce molecular hydrogen from water is receiving considerable attention, in an effort to decrease our reliance on fossil fuels. The prevention of the aggregation of active sites during material synthesis, in order to increase charge transport properties of electrocatalysts, is needed. We have designed, synthesized, and studied a Ag₂S/reduced graphene oxide (rGO) electrochemical catalyst (for hydrogen evolution) from water. The Ag₂S nanocrystals were synthesized by the solvothermal method in which the rGO was added. The addition of the rGO resulted in the formation of smaller Ag₂S nanocrystals, which consequently increased the electrical conductivity of the composite catalyst. The composite catalyst showed a higher electrochemical catalytic activity than the one with an absence of rGO. At a current density of 10 mA/cm², a low overpotential of 120 mV was obtained. A Tafel slope of 49.1 mV/dec suggests a Volmer–Herovskyy mechanism for the composite catalyst. These results may provide a novel strategy for developing hydrogen evolution reaction (HER) electrocatalysts, via the combining of a nano-semiconductor catalyst with a 2D material.

Keywords: HER; Ag₂S nanocrystals; reduced graphene oxide (rGO); electrocatalyst; composites

1. Introduction

Hydrogen is an energy carrier with the highest combustion heat known. When produced from a renewable source, it has no harmful environmental effect. Among the strategies for producing hydrogen, electrocatalytic water splitting is an efficient, green (if electricity originates from renewable sources), and potentially low-cost method.

Among various types of semiconductors, Ag₂S has recently attracted interest due to its negligible toxicity and broad absorption spectrum that extends into the near infrared. Bulk Ag₂S has a band gap of 1.06 ± 0.2 eV [1], which can be further adjusted to 1.44 eV through size-control or surface modification. Ag₂S has been studied because of its possible applications as a photodetector [2–4], as a photo-catalyst [5,6], in near-infrared fluorescence imaging in vivo [7–9], in surface-enhanced Raman scattering [10,11], and as a nanocrystal-sensitized solar cell [12–16]. In some work, nanomaterials,

including Ag₂S nanocrystals, have also been used for electrocatalytic reactions [17,18]. For example, Pande's group studied an Ag₂S-Ag heterostructure material as an electrocatalyst for the hydrogen evolution reaction (HER). They obtained an overpotential of 199 mV and a Tafel slope of 102 mV/dec. [19]. In our recent work, we have also carried out research on the electrochemical HER performance of Ag₂S nanocrystals, and obtained an overpotential of 320 mV and a Tafel slope of 86 mV/dec. [20].

The solution synthesis method has the obvious advantages of convenience, controllability, and a low cost. However, the aggregation problem, which has a serious adverse effect on the catalytic performance, is difficult to avoid in the solution synthesis method [21]. In order to address this problem, the introduction of two-dimensional (2D) materials, to improve the electrocatalytic performance, has been tried by several groups [22–32]. Wang's group used the Ag-Ag₂S/MoS₂ heterojunction as an electrocatalyst for HER and obtained an overpotential of 410 mV [33]. Rizzi's group used a waste Digital Video Disc (DVD) as a substrate and synthesized a photo-electrocatalyst for the hydrogen evolution reaction (HER) through the electrochemical deposition of MoS₂ on the Ag nanostructured surface of a commercial DVD. The composite material MoS₂/Ag₂S/Ag made was uniformly distributed n–p nanojunctions that performed better than those of the similar MoS₂-based systems. Both the conductivity of the substrate and the dispersion of the catalytic material were improved that way, which resulted in an overpotential of 121 mV and a Tafel slope of 41 mV/dec [34]. Reduced graphene oxide (rGO), as a 2D material, has many advantages, including a large specific surface area, a high concentration of step edges, and a capacity to be easily chemically modified [21]. It is, thus, potentially promising as a component for electrocatalysts. Some pioneering work has been conducted in designing composite catalyst systems, with promising results [22,23,30,35–40]. For example, Yu's group found Ag₂S/rGO to be an efficient catalyst for the reduction of 4-nitrophenol [41]. Compared to pure Ag₂S nanocrystals, a composite catalyst system is expected to have a higher electrocatalytic efficiency in the reduction of 4-nitrophenol. Alberto's group also explored the role of introducing Ag₂S nanocrystals in MoS₂/rGO catalysts. In addition, the catalytic performance was significantly improved, which can be derived from the decrease in overpotential and the Tafel slope [42].

In this work, we found that the Ag₂S/rGO composite, upon surface modification and with a suitable electronic band gap, can become an active and stable electrocatalyst for the HER. The electrochemical characterization of the composite catalyst was carried out, and the internal mechanism of its high electrocatalytic efficiency is discussed. The results indicate that in the composite catalyst, the Ag₂S size distribution decreased. In addition, the charge transfer property increased because of the increased conductivity. Therefore, the performance of the composite catalyst is improved, relative to the pure Ag₂S catalyst. We also calculated and compared the electrochemical catalytic performance of other catalysts containing Ag₂S and other semiconductor nanomaterials with rGO from existing literature (Figure S1). The composite Ag₂S/rGO catalyst, in this work, showed a considerable performance improvement.

2. Result and Discussion

The crystals of free Ag₂S nanocrystal are shown in Figure 1a; they have a mean particle size of about 15 nm. Figure 1b shows a TEM image of the GO, and the Ag₂S particles on top of rGO are shown in Figure 1c. Smaller aggregates of Ag₂S are present when the Ag₂S is deposited onto the rGO (mean particle size of about 7 nm). The results show that the presence of the rGO sheets prevented further growth of the Ag₂S nanocrystals during the synthesis. A high-resolution TEM (HRTEM) image of the Ag₂S nanocrystals on the rGO sheets is shown in Figure 1d. The lattice spacing of 0.16 and 0.19 nm corresponded to the spacing of the (141) and (212) faces of the Ag₂S, respectively.

The optical, diffraction, and vibrational characteristics of the Ag₂S/rGO composite are presented in Figure 2. The UV-Vis-IR absorbance spectra showed an onset at 880 nm (Figure 2a), from which the band gap was extracted to be ca. 1.4 eV. The first excitonic absorbance peak was located at 800 nm. The fluorescence spectra of the Ag₂S/rGO composite, Ag₂S/GO composite, Ag₂S, and GO are shown in Figure 2b. One can see a fluorescence centered at 825 nm in all three of the samples containing the Ag₂S nanocrystals (which corresponds to 1.5 eV). After the addition of the GO and rGO, the peak

position did not shift within the experimental errors (± 3 nm). A direct comparison between the PL and UV-vis absorbance may not be possible, particularly because of the presence of excitonic absorbance and quantum size effects. Figure S3 shows the changes in photoluminescence at the different ratios of Ag_2S to rGO; the decrease in the PL with the decreasing Ag_2S wt. % is due to the dilution effect, yet the trend is not linear. This might be due to experimental uncertainty but may also be evidence of some charge transfer between the Ag_2S and rGO. The XRD patterns of the $\text{Ag}_2\text{S}/\text{rGO}$ composite are given in Figure 2c; they matched well with its orthorhombic structure [7]. The black curve refers to the XRD reference card of the Ag_2S (PDF#03-0844).

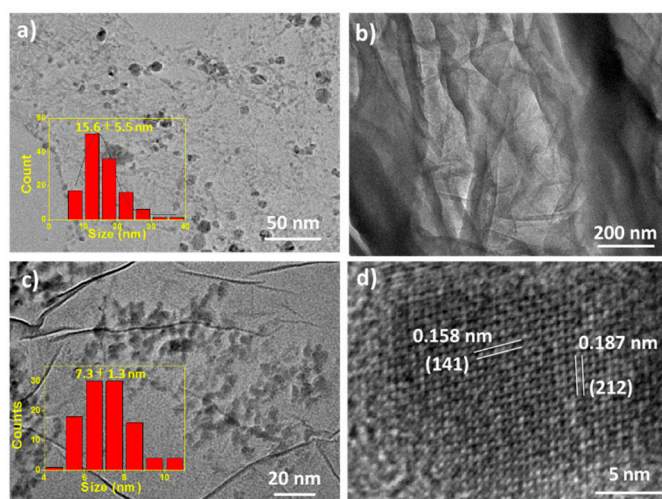


Figure 1. (a) A TEM image of free Ag_2S crystals, inset: a particle size distribution histogram. (b) A TEM image of a GO sheet. (c) A TEM image on $\text{Ag}_2\text{S}/\text{rGO}$, inset: a histogram of the particle size distribution of Ag_2S crystals. (d) A high-resolution TEM (HRTEM) image of the $\text{Ag}_2\text{S}/\text{rGO}$.

The dynamic measurements were performed using a time resolved photoluminescence (TRPL) system. Figure 2d shows TRPL spectra of the free Ag_2S and $\text{Ag}_2\text{S}/\text{rGO}$; the lifetime data are shown in Table S1. The fluorescence lifetime of the Ag_2S was found to be about 7.7 ns. It decreased by about half upon the deposition on rGO from 7.7 to 4.3 ns, which might be related to the increasing electron-hole pair separation due to the rapid charge transfer in $\text{Ag}_2\text{S}/\text{rGO}$. This might result in a more efficient H_2 elevating reaction on the surface of Ag_2S nanoparticle nanocrystals, and the interface between the Ag_2S nanocrystals and rGO.

The electrocatalytic behavior is shown in Figure 3. Experiments were carried out using a standard three-electrode system, in a 0.5 M H_2SO_4 aqueous solution. An overpotential of the $\text{Ag}_2\text{S}/\text{rGO}$ composite for HER (of about 120 mV) was obtained from the polarization curve, shown in Figure 3a. In contrast, the $\text{Ag}_2\text{S}/\text{GO}$ composite, Ag_2S , and rGO (used as the electrocatalysts) showed overpotentials of 131, 207, and 240 mV, respectively. The Tafel curves, extracted from the linear region of the polarization curves, are shown in Figure 3b. From the Tafel equation ($\eta = b \log j + a$, in which j is the current density and b is the Tafel slope), the slopes of the $\text{Ag}_2\text{S}/\text{rGO}$ composite, $\text{Ag}_2\text{S}/\text{GO}$ composite, Ag_2S , and rGO were found to be 49.1, 62.3, 99.2, and 120.6 mV/dec, respectively. The performance of catalysts mentioned above is listed in Table 1. The oscillation of the Tafel curve of the Ag_2S can be attributed to the moderate stability of the Ag_2S as an electrocatalyst. The polarization curve and the Tafel curve confirmed the improvement performance of the $\text{Ag}_2\text{S}/\text{rGO}$ composite catalyst.

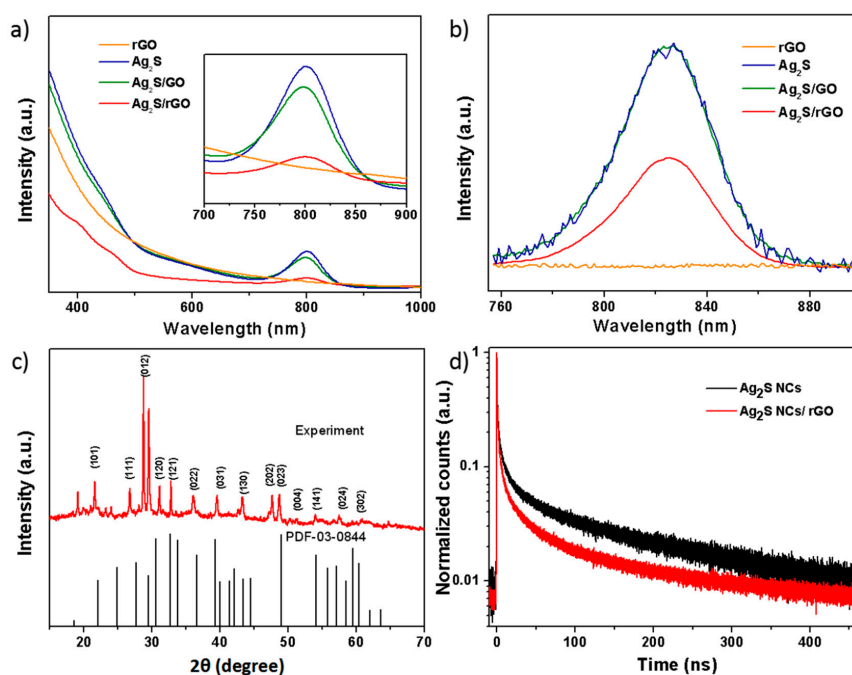


Figure 2. Optical and diffraction properties of the $\text{Ag}_2\text{S}/\text{rGO}$ composite series. (a) UV-Vis absorbance spectra of $\text{Ag}_2\text{S}/\text{rGO}$ composite series. (b) Photoluminescence spectra of the series at an excitation wavelength of 400 nm. (c) XRD patterns of the $\text{Ag}_2\text{S}/\text{rGO}$ composite. (d) Normalized time-resolved photoluminescence (PL) spectra recorded at the PL peak for the Ag_2S nanocrystals and $\text{Ag}_2\text{S}/\text{rGO}$ composite.

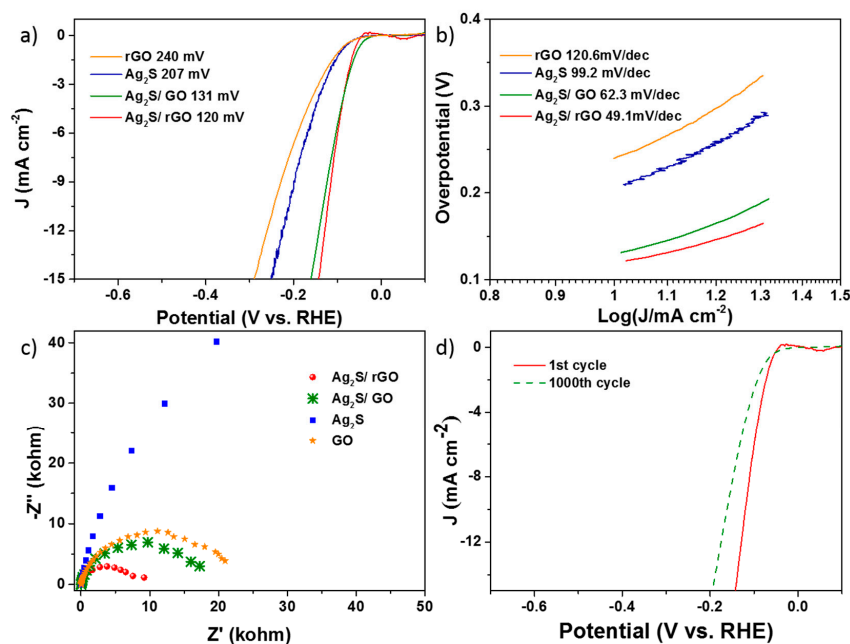


Figure 3. Electrocatalytic hydrogen evolution reaction (HER) performance. (a) Polarization curves recorded at a scanning speed of 20 mV/dec for $\text{Ag}_2\text{S}/\text{rGO}$, $\text{Ag}_2\text{S}/\text{GO}$, Ag_2S , and rGO. (b) The corresponding Tafel curves of the catalysts derived from (a,c) Potentiostatic electrochemical impedance spectroscopy (PEIS) Nyquist plots acquired at the overpotentials of $\text{Ag}_2\text{S}/\text{rGO}$, $\text{Ag}_2\text{S}/\text{GO}$, Ag_2S , and rGO obtained in (a,d) durability tests of $\text{Ag}_2\text{S}/\text{rGO}$ composite. Polarization curves were recorded before and after 1000 potential cycles in 0.5 M H_2SO_4 aqueous solution, from -2 to $+2$ V (vs. reversible hydrogen electrode (RHE)).

Table 1. Characteristics of Ag₂S/rGO for the HER.

Samples	Overpotential (mV)	Tafel Slope (mV/dec)
Ag ₂ S/rGO	120	49.1
Ag ₂ S/GO	131	62.3
Ag ₂ S	207	99.2
rGO	240	120.6

To further compare the samples, in particular, those of the Ag₂S/rGO and Ag₂S/GO, we measured the CV curves continuously for 1000 cycles. The polarization characteristics were tested before and after the 1000 cycles CV test, respectively, showing very small changes (Figure 3d). In addition, the typical CV scans (the 1st and 1000th) are shown in Figure S4a. The stability test of the Ag₂S/GO composite is shown in Figure S4b; it decreased much faster than that of the Ag₂S/rGO composite. The Ag₂S and rGO, alone, were unstable; they often fell off from the electrode and could not complete 1000 cycles during the CV test.

To further extrapolate the stability of the Ag₂S/rGO catalyst, XPS analysis before and after electro-catalytic reaction was carried out to investigate the possible compositional change of the Ag₂S/rGO (Figure 4 and Figure S5). The binding energy was calibrated with respect to the C1s (284.5 eV). Before the electrocatalytic reaction, the Ag 3d_{3/2} and Ag 3d_{5/2} were at 373.7 and 367.7 eV, respectively, which corresponded to the Ag⁺ cations in the Ag₂S [43–45]. After the electrocatalytic reaction, the Ag 3d_{3/2} and Ag 3d_{5/2} moved to 374.1 and 368.1 eV, respectively, which indicated the presence of Ag on the surface of the Ag₂S/rGO after the reaction [20]. As shown in Figure 4b, the peaks at 161.1 and 162.2 eV correspond to the S 2p of the Ag₂S, and the peaks at 162.0 and 163.3 eV correspond to the S 2p of the C–S in the MPA ligand. After the electrocatalytic reaction, the peak intensity of the S–C decreased, which might have been caused by the oxidation of the ligand [5,46,47]. The details of the fitting peaks of S before and after the HER reaction are listed in Tables 2 and 3, respectively. The atomic ratio of the Ag/S changed slightly from 1/1.94 to 1/1.86, which further proves the stability of the Ag₂S/rGO after the electrocatalytic reaction.

Table 2. Details of the fitting peaks of S before the HER reaction.

Peak	Binding Energy (BE) Position (eV)	Full Width Half Maximum (FWHM) (eV)	ΔE (eV)	Peak Area	% Lorentzian–Gaussian
1	161.1 2p _{3/2}	0.77	1.1	10,802	
2	162.0 2p _{3/2}	0.92	1.3	8041	
3	162.2 2p _{1/2}	0.90		5522	22%
4	163.3 2p _{1/2}	1.10		4135	

Table 3. Details of the fitting peaks of S after the HER reaction.

Peak	BE Position (eV)	FWHM (eV)	ΔE (eV)	Peak Area	% Lorentzian–Gaussian
1	161.2 2p _{3/2}	0.73	1.0	9566	
2	162.0 2p _{3/2}	0.91	1.4	1207	
3	162.2 2p _{1/2}	0.90		5034	21%
4	163.4 2p _{1/2}	0.99		589	

We then further explored the reasons for the higher activity of the Ag₂S/rGO composite catalysts for HER. This higher performance may be attributed to three points: (i) the Ag₂S nanocrystals grown on the surface of the rGO were better dispersed than the free-grown Ag₂S nanocrystals; (ii) the sizes of the Ag₂S nanocrystals on the rGO were slightly smaller, which may have had a different intrinsic electrocatalytic activity; and (iii) rGO can have an enhanced conductivity compared to Ag₂S alone, which would lead to less electrochemical impedance than that in the other samples (Figure 3c).

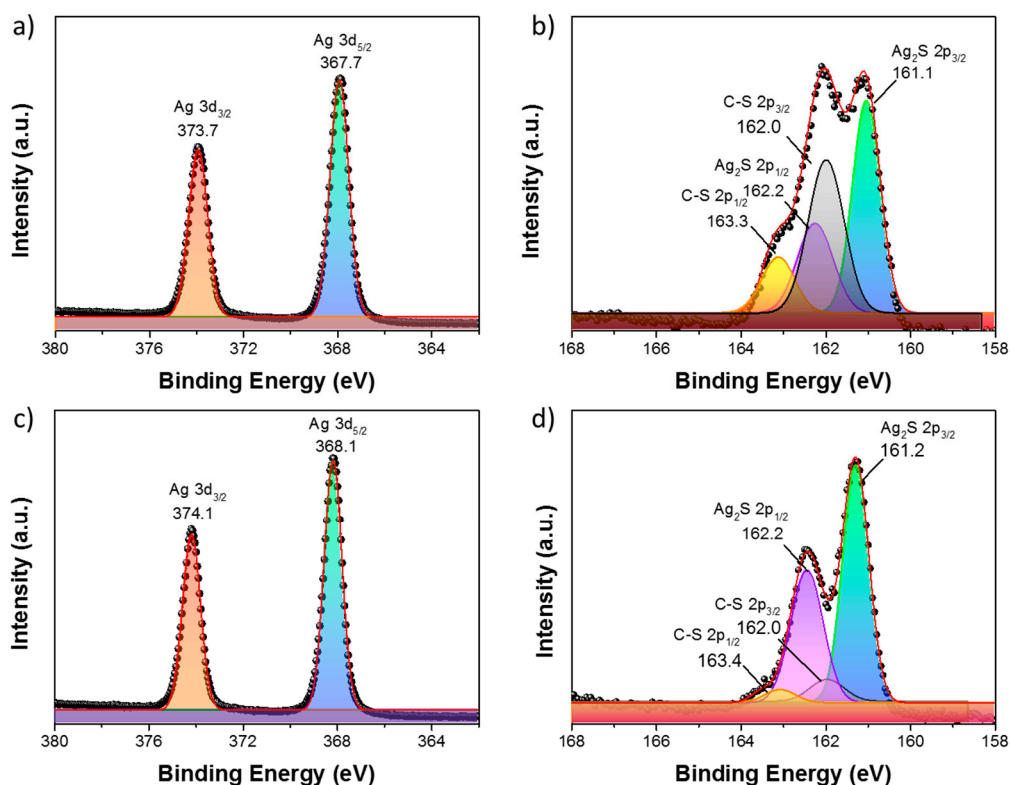
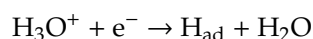


Figure 4. XPS spectra of Ag 3d (a,c) and S 2p (b,d). Elements from Ag₂S/rGO measured before (a,b) and after (c,d) electrochemical cyclic voltammetry (CV) test.

In the presence of the rGO, the free electrons generated on the Ag₂S nanocrystals may be transferred to the rGO [48]. The proton interaction and further hydrogen evolution reaction are enhanced because the rGO provides the needed large surface area. At the same time, it does not block the active sites on the Ag₂S nanocrystals' surfaces, meaning it can continue generating the electrons needed for the hydrogen evolution reaction. In the absence of an rGO substrate, all the reactions would be carried out on the surface of the Ag₂S nanocrystals. It is, thus, plausible that a synergistic effect between the Ag₂S nanocrystals and rGO is present, leading to an improvement in the efficiency of molecular hydrogen production.

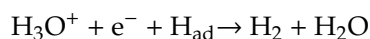
Three processes may occur in the electrocatalytic HER, in the acidic electrolytic condition. Firstly, the hydrated protons are combined with electrons (e⁻) and then form an adsorbed hydrogen (H_{ad})—where ad stands for adsorbed (the Volmer reaction) [18,49]:



$$b = \frac{2.3 RT}{\alpha F} \approx 120 \text{ mV/dec}$$

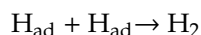
where R is the ideal gas constant, T is the absolute temperature, α is the symmetry coefficient (approximately equal to 0.5), and F is the Faraday constant. Following the first step, two possible reactions for H₂ production may occur: an electrochemical desorption reaction (Heyrovsky reaction) or a recombination reaction (Tafel reaction).

In the Heyrovsky reaction, the H_{ad} combines with a second hydrated protons and a second electron from the catalyst to form a hydrogen molecule:



$$b = \frac{2.3 RT}{(1 + \alpha)F} \approx 40 \text{ mV/dec}$$

In the Tafel reaction, two H_{ad} directly combine to form a hydrogen molecule:



$$b = \frac{2.3 RT}{2F} \approx 30 \text{ mV/dec}$$

In the case of the Ag_2S/rGO -catalyzed electrochemical HER reaction, two processes may occur, as shown in Figure 5. The Volmer process may occur on both the Ag_2S and rGO. The adsorbed hydrogen was formed on the surface of the catalysts waiting for the next reaction process. The Tafel slope was found to be equal, 49 and 120 mV/dec for the Ag_2S/rGO and rGO, respectively. Thus, the reaction on the surface of the Ag_2S/rGO , here, can be determined following the Volmer–Herovskiy mechanism [48,49]. The decrease in the Tafel slope of the Ag_2S/rGO composite (49 mV/dec), relative to that of the free Ag_2S nanocrystals (99 mV/dec) and Ag_2S/GO composite (63 mV/dec), can be attributed to the improvement in two steps, in the presence of rGO. The Ag_2S nanocrystals grown on the rGO were more uniform and of smaller size than the free Ag_2S nanocrystals, which provided more active sites for the adsorption of the protons and, therefore, the generation of molecular hydrogen. The better charge transfer ability of the rGO facilitated the electrical coupling between the Ag_2S nanocrystals and the underlying rGO sheets.

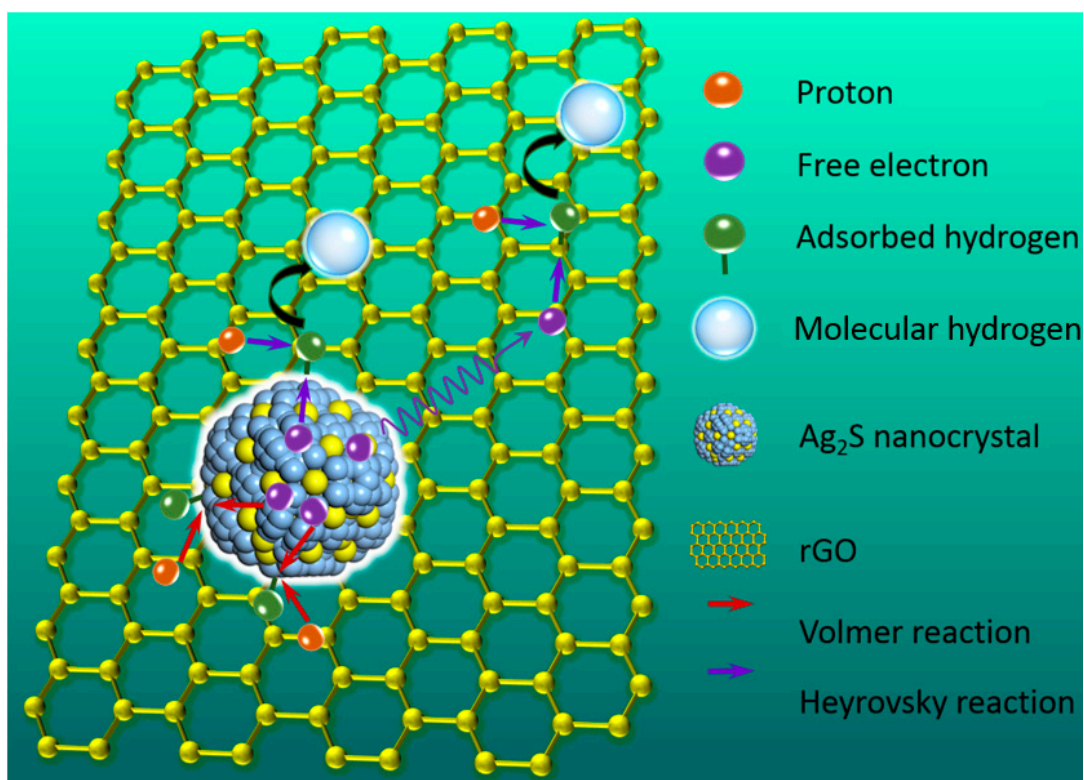


Figure 5. The HER reaction catalyzed by Ag_2S/rGO .

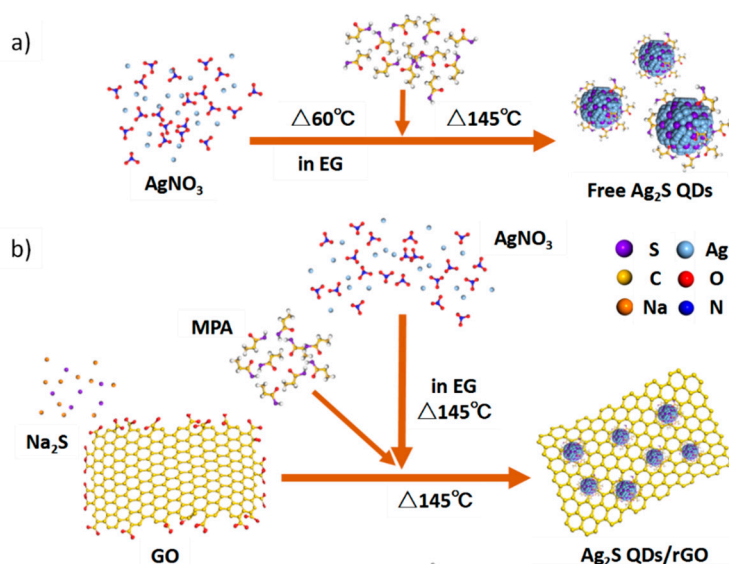
3. Experimental

3.1. Chemicals and Materials

The $AgNO_3$ powder and ethylene glycol (EG) were purchased from Sinopharm Chemical Reagent Co., Ltd. Shanghai, China. The 3-mercaptopropionic acid was purchased from Shanghai Aladdin Biochemical Technology Co., Ltd., Shanghai, China. The Na_2S was purchased from Beijing Chemical Works, Beijing, China. The GO and electrochemical adhesive Nafion were purchased from Sigma Aldrich Co., Ltd., St. Louis, MO, the United States.

3.2. Synthesis of Ag₂S Nanocrystals

Fifty-one milligrams of AgNO₃ was dissolved in 90 mL of ethylene glycol (EG) under nitrogen at 60 °C, as shown in Scheme 1a. Then, 0.06 mL (7 mmol) of 3-mercaptopropionic acid (MPA) was added. The mixture was stirred vigorously for 10 min and then heated to 145 °C. The solution color changed from a white to yellow clarification. After the reaction was finished, the solution was cooled to room temperature. The product was separated by centrifugation, then dispersed in the deionized water. The free Ag₂S nanocrystals were obtained.



Scheme 1. Schematic representation of the synthesis of Ag₂S nanocrystals in ethylene glycol (EG) solution without and with reduced graphene oxide (rGO) sheets. (a) Schematic solvothermal synthesis of the free Ag₂S. (b) Schematic solvothermal synthesis with rGO sheets, used for the Ag₂S/rGO composite.

3.3. Synthesis of Ag₂S/rGO Composite

The method of synthesizing Ag₂S/rGO is presented in Scheme 1b. Fifty-one milligrams of AgNO₃ was dissolved in 90 mL of ethylene glycol (EG) under nitrogen at 60 °C. Then, 0.06 mL (0.7 mmol) of 3-mercaptopropionic acid (MPA) was added. The mixture was stirred vigorously for 10 min, then heated to 145 °C. The reaction solution changed from white to yellow. Two milliliters (0.1 M) of the Na₂S aqueous solution and 2.325 mL (4 mg/mL) of the GO were quickly injected into the mixture. The Na₂S was added together with the GO as a reducing agent. After the reaction was finished, the solution was cooled to room temperature. The product was separated through centrifugation, then dispersed in the deionized water.

In the thus-synthesized Ag₂S/rGO composite, Ag₂S nanocrystals were uniformly distributed in the rGO according to the EDS spectra of the Ag₂S/rGO composite, shown in Figure S2. The size of the GO is on the micrometer scale, as shown in Scheme 1a.

3.4. Characterizations

The microstructure of the composite was characterized with a TEM (H-800 electron microscope with a charged coupled device camera with a 200 kV acceleration voltage). The high-resolution TEM (HRTEM) image was recorded with a JEM-2100F electron microscope at 200 kV. The energy dispersive analysis (EDX) of the composite catalyst was performed through the Phenom Element Identification application, attached to the Phenom Pro-X, at room temperature. The X-ray photoelectron spectra (XPS) were recorded with the Thermo Scientific Escalab 250Xi, Thermo Fisher Scientific (China) Co., Ltd., Shanghai, China. The crystal structure of the composite was obtained from X-ray diffraction (XRD) spectra recorded using a BRUKER D8 FOCUS, Bruker Daltonics Inc. that was operated

in air at room temperature. The photoluminescence and UV-Vis spectra were recorded using a fluorescence spectrometer (a Cary Eclipse Fluorescence Spectrophotometer from Agilent Technologies Inc., Santa Clara, CA, USA) and a Cary 100 Conc UV-Vis spectrophotometer, respectively, in air at room temperature. A self-made dynamic fluorescence system was used for the fluorescence lifetime. The tests were carried out on a solution dropped onto a glass slide. The excitation light was a 532 nm picosecond laser, with a repetition rate of 2 MHz. Each sample was tested at five different locations; the results are listed in Table S2.

3.5. Electrochemical HER Performance Test

The electrocatalytic HER reactions were carried out on a standard three-electrode biologic electrochemical workstation (VMP3), which was assembled using a Rotating Ring Disk Electrode (RRDE) apparatus at room temperature. For the Ag₂S and Ag₂S/rGO catalysts, 10 mg of powder was dispersed in 1 mL of a deionized water/ethanol mixture (= 1:1). Then, 50 µL of 5 wt% of Nafion 117 was added and followed by ultra-sonication. Five microliters of the as-prepared material was then pipetted onto a glassy carbon electrode (GCE) with an effective area of 0.07065 cm² and dried. Thus, the catalyst loaded onto the GCE was about 0.708 mg/cm². For the GO and rGO catalysts, 50 µL of 5 wt% of Nafion 117 was added into 1 mL of the 4 mg/mL aqueous solution and followed by ultra-sonication. Then, 12.5 µL (divided into two: 6 µL and 6.5 µL) of the as-prepared material was pipetted onto the GCE, then dried. Thus, the catalyst loaded onto the GCE was about 0.708 mg/cm². The electrolyte was a 0.5 M aqueous solution of sulfuric acid. Using a saturated calomel electrode as a reference electrode (and a platinum wire as a counter electrode), the cyclic voltammeteries (CVs) were tested from −2 to 2 V, with a scanning speed of 100 mV/s. The polarization curves were acquired within a range of −0.7 V to 0 V, and at a scanning speed of 20 mV/s. The Nyquist plots of the composite were tested from 100 kHz to 0.01 Hz. The stability tests were carried out by comparing the polarization curves before and after 1000 cycles of the voltammograms cycle.

4. Conclusions

Introducing the rGO micro-sheets by the solvothermal method improves the electrocatalytic (HER) activity of the Ag₂S nanocrystals. A Tafel slope of 49.1 mV/dec and an overpotential of 120 mV were obtained for the Ag₂S/rGO composite electrocatalysts. Compared to the free Ag₂S nanocrystals and the Ag₂S/GO, the Ag₂S/rGO composite showed better dispersion and a uniform size distribution. The rGO also enhanced the electrocatalyst conductivity (PEIS Nyquist plots), as well as the charge transfer efficiency (the TR luminescence). The hydrogen production mechanism of the composite catalyst was found to follow the Volmer–Herovskiy mechanism. This work may provide a new strategy for developing active HER electrocatalysts, via the combining of a semiconductor with 2D materials.

Supplementary Materials: The following are available online at <http://www.mdpi.com/2073-4344/10/9/948/s1>. Electrochemical performance of the different catalysts (Figure S1); EDS of Ag₂S/rGO hybrid on the glass substrate (Figure S2); Changes in the photoluminescence at the different ratios of Ag₂S to rGO (Figure S3); Stability performance of the Ag₂S/GO hybrid (Figure S4); Survey XPS spectrum of Ag₂S/rGO before and after the electrocatalyst reaction (Figure S5); Tauc plot for Ag₂S/rGO, Ag₂S/GO, and Ag₂S—used for determining the band gaps (Figure S6); Fluorescence lifetime of Ag₂S and Ag₂S/rGO (Table S1); Performance of the rGO-based chalcogenide metal semiconductor composites as an electrocatalyst for the hydrogen evolution reaction (Table S2).

Author Contributions: The manuscript was written with contributions from all the authors. C.Z. designed the research plan, implemented experiments including sample preparation, characterization and catalytic performance testing, conducted data analysis, and wrote the manuscript. Z.Y., J.X., and Y.Z. gave experimental help in the optical characterization of samples, including absorption spectra and fluorescence spectra. H.L. and H.Z. gave experimental help in the morphology characterization (TEM and HRTEM) of samples. W.Y., H.L., and C.G. gave guidance in experimental design, article writing and article revision. All authors have read and agreed to the published version of the manuscript.

Funding: This research was funded by the National Key Research and Development Program of China grant number 2018YFB1107202, 2017YFB1104700, National Natural Science Foundation of China grant number 91750205, 61774155, 51102107, & 21404015, the K. C. Wong Education Foundation grant number GJTD-2018-08, the Open Project of State Key Laboratory of Supramolecular Structure and Materials grant number sklssm202034, Bill and Melinda Gates Foundation grant number INV-009181.

Conflicts of Interest: The authors declare no conflict of interest.

References

1. Huxter, V.M.; Mirkovic, T.; Nair, P.S.; Scholes, G.D. Demonstration of bulk semiconductor optical properties in processable Ag₂S and EuS nanocrystalline systems. *Adv. Mater.* **2008**, *20*, 2439–2443. [[CrossRef](#)]
2. Chen, D.; Wei, L.; Wang, D.; Chen, Y.X.; Tian, Y.F.; Yan, S.S.; Mei, L.M.; Jiao, J. Ag₂S/ZnO core-shell nanoheterojunction for a self-powered solid-state photodetector with wide spectral response. *J. Alloys Compd.* **2018**, *735*, 2491–2496. [[CrossRef](#)]
3. Tang, S.L.; He, C.S.; Li, D.; Cai, W.H.; Fan, L.Z.; Li, Y.C. Precursor reactivity differentiation for single-step preparation of Ag₂Se@Ag₂S core-shell nanocrystals with distinct absorption and emission properties enabling sensitive near-infrared photodetection. *J. Mater. Sci.* **2018**, *53*, 11355–11366. [[CrossRef](#)]
4. Kang, M.H.; Kim, S.H.; Jang, S.; Lim, J.E.; Chang, H.; Kong, K.J.; Myung, S.; Park, J.K. Synthesis of silver sulfide nanoparticles and their photodetector applications. *RSC Adv.* **2018**, *8*, 28447–28452. [[CrossRef](#)]
5. Ghafoor, S.; Ata, S.; Mahmood, N.; Arshad, S.N. Photosensitization of TiO₂ nanofibers by Ag₂S with the synergistic effect of excess surface Ti³⁺ states for enhanced photocatalytic activity under simulated sunlight. *Sci. Rep.* **2017**, *7*, 255. [[CrossRef](#)]
6. Jiang, Y.; Liu, D.; Yang, Y.; Xu, R.; Zhang, T.; Sheng, K.; Song, H. Photoelectrochemical detection of alpha-fetoprotein based on ZnO inverse opals structure electrodes modified by Ag₂S nanoparticles. *Sci. Rep.* **2016**, *6*, 38400. [[CrossRef](#)]
7. Jiang, P.; Zhu, C.N.; Zhang, Z.L.; Tian, Z.Q.; Pang, D.W. Water-soluble Ag₂S quantum dots for near-infrared fluorescence imaging in vivo. *Biomaterials* **2012**, *33*, 5130–5135. [[CrossRef](#)]
8. Hong, G.; Robinson, J.T.; Zhang, Y.; Diao, S.; Antaris, A.L.; Wang, Q.; Dai, H. In vivo fluorescence imaging with Ag₂S quantum dots in the second near-infrared region. *Angew. Chem.* **2012**, *51*, 9818–9821. [[CrossRef](#)]
9. Hong, G.; Antaris, A.L.; Dai, H. Near-infrared fluorophores for biomedical imaging. *Nat. Biomed. Eng.* **2017**, *1*, 0010. [[CrossRef](#)]
10. Hou, X.; Zhang, X.; Yang, W.; Liu, Y.; Zhai, X. Synthesis of SERS active Ag₂S nanocrystals using oleylamine as solvent, reducing agent and stabilizer. *Mater. Res. Bull.* **2012**, *47*, 2579–2583. [[CrossRef](#)]
11. Fu, X.; Jiang, T.; Zhao, Q.; Yin, H. Charge-transfer contributions in surface-enhanced Raman scattering from Ag, Ag₂S and Ag₂Se substrates. *J. Raman Spectrosc.* **2012**, *43*, 1191–1195. [[CrossRef](#)]
12. Xue, J.; Liu, J.X.; Mao, S.; Wang, Y.; Shen, W.F.; Wang, W.; Huang, L.J.; Li, H.L.; Tang, J.G. Recent progress in synthetic methods and applications in solar cells of Ag₂S quantum dots. *Mater. Res. Bull.* **2018**, *106*, 113–123. [[CrossRef](#)]
13. Karimipour, M.; Bagheri, M.; Johansson, E.M.J.; Molaei, M. Excellent growth of ZnS shell on Ag₂S QDs using a photochemical-microwave irradiation approach and fabrication of their indoor QD thin film solar cells. *Mater. Technol.* **2018**, *33*, 784–792. [[CrossRef](#)]
14. Öberg, V.; Zhang, X.; Johansson, M.; Johansson, E. Solution-Processed Environmentally Friendly Ag₂S Colloidal Quantum Dot Solar Cells with Broad Spectral Absorption. *Appl. Sci.* **2017**, *7*, 1020. [[CrossRef](#)]
15. Suarez, J.A.; Plata, J.J.; Marquez, A.M.; Sanz, J.F. Ag₂S Quantum Dot-Sensitized Solar Cells by First Principles: The Effect of Capping Ligands and Linkers. *J. Phys. Chem. A* **2017**, *121*, 7290–7296. [[CrossRef](#)]
16. Cheng, L.Y.; Ding, H.M.; Chen, C.H.; Wang, N.N. Ag₂S/Bi₂S₃ co-sensitized TiO₂ nanorod arrays prepared on conductive glass as a photoanode for solar cells. *J. Mater. Sci. Mater. Electron.* **2016**, *27*, 3234–3239. [[CrossRef](#)]
17. Zilio, P.; Dipalo, M.; Tantussi, F.; Messina, G.C.; de Angelis, F. Hot electrons in water: Injection and ponderomotive acceleration by means of plasmonic nanoelectrodes. *Light Sci. Appl.* **2017**, *6*, e17002. [[CrossRef](#)]
18. Jiao, Y.; Zheng, Y.; Jaroniec, M.; Qiao, S.Z. Design of electrocatalysts for oxygen- and hydrogen-involving energy conversion reactions. *Chem. Soc. Rev.* **2015**, *44*, 2060–2086. [[CrossRef](#)]

19. Basu, M.; Nazir, R.; Mahala, C.; Fageria, P.; Chaudhary, S.; Gangopadhyay, S.; Pande, S. Ag₂S/Ag Heterostructure: A Promising Electrocatalyst for the Hydrogen Evolution Reaction. *ACS J. Surf. Colloid.* **2017**, *33*, 3178–3186. [[CrossRef](#)]
20. Yu, W.; Yin, J.; Li, Y.; Lai, B.; Jiang, T.; Li, Y.; Liu, H.; Liu, J.; Zhao, C.; Singh, S.C.; et al. Ag₂S Quantum Dots as an Infrared Excited Photocatalyst for Hydrogen Production. *ACS Appl. Energy Mater.* **2019**, *2*, 2751–2759. [[CrossRef](#)]
21. Chen, Y.; Yang, K.; Jiang, B.; Li, J.; Zeng, M.; Fu, L. Emerging two-dimensional nanomaterials for electrochemical hydrogen evolution. *J. Mater. Chem. A* **2017**, *5*, 8187–8208. [[CrossRef](#)]
22. Zhang, Y.F.; Yang, J.; Dong, Q.C.; Geng, H.B.; Zheng, Y.; Liu, Y.L.; Wang, W.J.; Li, C.C.; Dong, X.C. Highly Dispersive MoP Nanoparticles Anchored on Reduced Graphene Oxide Nanosheets for an Efficient Hydrogen Evolution Reaction Electrocatalyst. *ACS Appl. Mater. Interfaces* **2018**, *10*, 26258–26263. [[CrossRef](#)] [[PubMed](#)]
23. Ravula, S.; Zhang, C.; Essner, J.; Robertson, J.; Lin, J.; Baker, G. Ionic liquid-assisted synthesis of nanoscale (MoS₂)_x(SnO₂)_{1-x} on reduced graphene oxide for the electrocatalytic hydrogen evolution reaction. *ACS Appl. Mater. Interfaces* **2017**, *9*, 8065–8074. [[CrossRef](#)] [[PubMed](#)]
24. Pham, C.V.; Zana, A.; Arenz, M.; Thiele, S. [Mo₃S₁₃]₂- Cluster Decorated Sulfur-doped Reduced Graphene Oxide as Noble Metal-Free Catalyst for Hydrogen Evolution Reaction in Polymer Electrolyte Membrane Electrolyzers. *Chemelectrochem* **2018**, *5*, 2672–2680. [[CrossRef](#)]
25. Fu, H.Y.; Chen, Y.J.; Ren, Z.Y.; Xiao, Y.T.; Liu, Y.Y.; Zhang, X.; Tian, G.H. Highly dispersed of Ni_{0.85}Se nanoparticles on nitrogen-doped graphene oxide as efficient and durable electrocatalyst for hydrogen evolution reaction. *Electrochim. Acta* **2018**, *262*, 107–114. [[CrossRef](#)]
26. Cho, J.S.; Park, S.K.; Jeon, K.M.; Piao, Y.; Kang, Y.C. Mesoporous reduced graphene oxide/WSe₂ composite particles for efficient sodium-ion batteries and hydrogen evolution reactions. *Appl. Surf. Sci.* **2018**, *459*, 309–317. [[CrossRef](#)]
27. Yang, Y.Y.; Li, F.; Li, W.Z.; Gao, W.B.; Wen, H.; Li, J.; Hu, Y.P.; Luo, Y.T.; Li, R. Porous CoS₂ nanostructures based on ZIF-9 supported on reduced graphene oxide: Favourable electrocatalysis for hydrogen evolution reaction. *Int. J. Hydrogen Energy* **2017**, *42*, 6665–6673. [[CrossRef](#)]
28. Tan, S.M.; Pumera, M. Electrosynthesis of Bifunctional WS_{3-x}/Reduced Graphene Oxide Hybrid for Hydrogen Evolution Reaction and Oxygen Reduction Reaction Electrocatalysis. *Chem. Eur. J.* **2017**, *23*, 8510–8519. [[CrossRef](#)]
29. Sun, W.Y.; Li, P.; Liu, X.; Shi, J.J.; Sun, H.M.; Tao, Z.L.; Li, F.J.; Chen, J. Size-controlled MoS₂ nanodots supported on reduced graphene oxide for hydrogen evolution reaction and sodium-ion batteries. *Nano Res.* **2017**, *10*, 2210–2222. [[CrossRef](#)]
30. Liu, Y.R.; Shang, X.; Gao, W.K.; Dong, B.; Li, X.; Li, X.H.; Zhao, J.C.; Chai, Y.M.; Liu, Y.Q.; Liu, C.G. In situ sulfurized CoMoS/CoMoO₄ shell-core nanorods supported on N-doped reduced graphene oxide (NRGO) as efficient electrocatalyst for hydrogen evolution reaction. *J. Mater. Chem. A* **2017**, *5*, 2885–2896. [[CrossRef](#)]
31. Li, C.X.; Grantham, J.; Zhao, W. One-pot growth of 3D reduced graphene oxide foams embedded with MoS₂ and Ni-doped MoS₂ nanocatalysts for hydrogen evolution reaction. *Abstr. Pap. Am. Chem. Soc.* **2017**, *253*, 3158–3163.
32. Lee, J.E.; Jung, J.; Ko, T.Y.; Kim, S.; Kim, S.I.; Nah, J.; Ryu, S.; Nam, K.T.; Lee, M.H. Catalytic synergy effect of MoS₂/reduced graphene oxide hybrids for a highly efficient hydrogen evolution reaction. *RSC Adv.* **2017**, *7*, 5480–5487. [[CrossRef](#)]
33. Xia, X.H.; Zhao, X.J.; Ye, W.C.; Wang, C.M. Highly porous Ag-Ag₂S/MoS₂ with additional active sites synthesized by chemical etching method for enhanced electrocatalytic hydrogen evolution. *Electrochim. Acta* **2014**, *142*, 173–181. [[CrossRef](#)]
34. Kosmala, T.; Mosconi, D.; Giallongo, G.; Rizzi, G.A.; Granozzi, G. Highly Efficient MoS₂/Ag₂S/Ag Photoelectrocatalyst Obtained from a Recycled DVD Surface. *ACS Sustain. Chem. Eng.* **2018**, *6*, 7818–7825. [[CrossRef](#)]
35. Liu, X.X.; Zang, J.B.; Chen, L.; Chen, L.B.; Chen, X.; Wu, P.; Zhou, S.Y.; Wang, Y.H. A microwave-assisted synthesis of CoO@Co core-shell structures coupled with N-doped reduced graphene oxide used as a superior multi-functional electrocatalyst for hydrogen evolution, oxygen reduction and oxygen evolution reactions. *J. Mater. Chem. A* **2017**, *5*, 5865–5872. [[CrossRef](#)]

36. Qin, Y.C.; Dai, X.P.; Zhang, X.; Huang, X.L.; Sun, H.; Gao, D.W.; Yu, Y.B.; Zhang, P.F.; Jiang, Y.; Zhuo, H.Y.; et al. Microwave-assisted synthesis of multiply-twinned Au-Ag nanocrystals on reduced graphene oxide for high catalytic performance towards hydrogen evolution reaction. *J. Mater. Chem. A* **2016**, *4*, 3865–3871. [[CrossRef](#)]
37. Konkena, B.; Masa, J.; Xia, W.; Muhler, M.; Schuhmann, W. MoSSe@reduced graphene oxide nanocomposite heterostructures as efficient and stable electrocatalysts for the hydrogen evolution reaction. *Nano Energy* **2016**, *29*, 46–53. [[CrossRef](#)]
38. Akyuz, D.; Keskin, B.; Sahinturk, U.; Koca, A. Electrocatalytic hydrogen evolution reaction on reduced graphene oxide electrode decorated with cobaltphthalocyanine. *Appl. Catal. B Environ.* **2016**, *188*, 217–226. [[CrossRef](#)]
39. Yan, H.J.; Tian, C.G.; Wang, L.; Wu, A.P.; Meng, M.C.; Zhao, L.; Fu, H.G. Phosphorus-Modified Tungsten Nitride/Reduced Graphene Oxide as a High-Performance, Non-Noble-Metal Electrocatalyst for the Hydrogen Evolution Reaction. *Angew. Chem. Int. Ed.* **2015**, *54*, 6325–6329. [[CrossRef](#)]
40. Ma, L.B.; Shen, X.P.; Zhou, H.; Zhu, G.X.; Ji, Z.Y.; Chen, K.M. CoP nanoparticles deposited on reduced graphene oxide sheets as an active electrocatalyst for the hydrogen evolution reaction. *J. Mater. Chem. A* **2015**, *3*, 5337–5343. [[CrossRef](#)]
41. Lang, B.; Yu, H.-K. Novel Ag₂S nanoparticles on reduced graphene oxide sheets as a super-efficient catalyst for the reduction of 4-nitrophenol. *Chin. Chem. Lett.* **2017**, *28*, 417–421. [[CrossRef](#)]
42. Solomon, G.; Mazzaro, R.; You, S.; Natile, M.M.; Morandi, V.; Concina, I.; Vomiero, A. Ag₂S/MoS₂ Nanocomposites Anchored on Reduced Graphene Oxide: Fast Interfacial Charge Transfer for Hydrogen Evolution Reaction. *ACS Appl. Mater. Interfaces* **2019**, *11*, 22380–22389. [[CrossRef](#)] [[PubMed](#)]
43. Ren, H.T.; Xu, W.C.; Zhu, S.L.; Cui, Z.D.; Yang, X.J.; Inoue, A. Synthesis and properties of nanoporous Ag₂S/CuS catalyst for hydrogen evolution reaction. *Electrochim. Acta* **2016**, *190*, 221–228. [[CrossRef](#)]
44. Aazam, E.S. Photocatalytic oxidation of methylene blue dye under visible light by Ni doped Ag₂S nanoparticles. *J. Ind. Eng. Chem.* **2014**, *20*, 4033–4038. [[CrossRef](#)]
45. Romand, M.; Roubin, M.; Deloume, J.P. ESCA studies of some copper and silver selenides. *J. Electron Spectrosc. Relat. Phenom.* **1978**, *13*, 229–242. [[CrossRef](#)]
46. Kaushik, V.K. XPS core level spectra and Auger parameters for some silver compounds. *J. Electron Spectrosc. Relat. Phenom.* **1991**, *57*, 273–277. [[CrossRef](#)]
47. Siriwardane, R.V.; Cook, J.M. Interactions of NO and SO₂ with iron deposited on silica. *J. Colloid Interface Sci.* **1985**, *104*, 250–257. [[CrossRef](#)]
48. Chen, D.J.; Zou, L.L.; Li, S.X.; Zheng, F.Y. Nanospherical like reduced graphene oxide decorated TiO₂ nanoparticles: An advanced catalyst for the hydrogen evolution reaction. *Sci. Rep.* **2016**, *6*, 20335. [[CrossRef](#)]
49. Wang, J.; Xu, F.; Jin, H.; Chen, Y.; Wang, Y. Non-Noble Metal-based Carbon Composites in Hydrogen Evolution Reaction: Fundamentals to Applications. *Adv. Mater.* **2017**, *29*, 1605838. [[CrossRef](#)]

